ACS Catalysis
Research Article
pubs.acs.org/acscatalysis

High Activity of Au/γ-Fe_2O_3 for CO Oxidation: Effect of Support Crystal Phase in Catalyst Design

Kunfeng Zhao,[†,§,#,∥] Hailian Tang,[†,§,‡,#] Botao Qiao,[*,†] Lin Li,[†] and Junhu Wang[*,†,§]

[†]State Key Laboratory of Catalysis, Dalian Institute of Chemical Physics, Chinese Academy Sciences, Dalian 116023, China
[§]Mössbauer Effect Data Center & Laboratory of Catalysts and New Materials for Aerospace, Dalian Institute of Chemical Physics, Chinese Academy of Sciences, Dalian 116023, China
[‡]University of Chinese Academy of Sciences, Beijing 100049, China

Supporting Information

ABSTRACT: Au/γ-Fe_2O_3 and Au/α-Fe_2O_3 catalysts with identical size of Au nanoparticles, chemical state of Au species, and amount of surface OH^- group were prepared. The Au/γ-Fe_2O_3 catalyst exhibited exceptionally high activity, regardless of the heat treatments. The CO-TPR, sequential pulse reaction, and in situ Raman spectra demonstrate that the much higher activity of Au/γ-Fe_2O_3 originated from its higher redox property at low temperature. Systematic study shows that this higher-redox-property-based higher activity could be extended to γ-Fe_2O_3-supported Pt-group metals and to other reactions that follow Mars−Van Krevelen mechanism. This finding may provide a new avenue for catalyst improvement or development by choosing the suitable crystal phase of the oxide support.

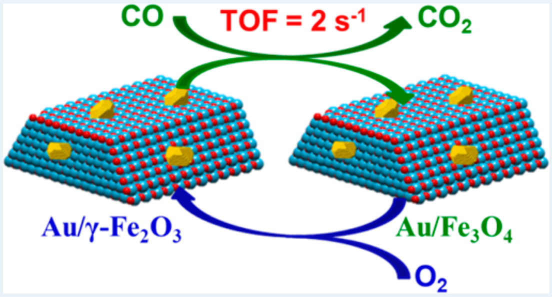

KEYWORDS: *gold, CO oxidation, redox, γ-Fe_2O_3, catalyst design*

INTRODUCTION

Heterogeneous catalysis is critical for many important industrial processes and environmental issues that are closely related to our daily life.[1,2] The demand to develop new catalytic materials may be endless due to our continuous pursuit of better catalytic performance (e.g., higher activity/selectivity and better stability, affordability, and abundant elements, etc.) or of new and green catalytic processes.[3] Finding the right catalytic materials, however, has many elements of trial and error and thus is usually a tedious, time-consuming process.[4,5] Therefore, the catalyst development by rational design has been a long-term dream and is regarded as one of the greatest challenges.[3,5,6]

In the past decades, oxides-supported gold nanoparticles (NPs) or clusters as catalysts have attracted a great deal of and yet increasing interest in the catalysis field. On the one hand, supported Au catalysts have demonstrated unique catalytic performance for numerous important chemical reactions.[7−12] On the other hand, the performances of supported Au catalysts were dramatically influenced by many factors such as the size of gold NPs, the valence state of the gold, and the nature of the support oxides as well as the interaction between gold and them. The latter is not only fundamentally interesting but also practically important because an in-depth understanding of why and how these factors influence the catalyst could be helpful to modify the catalyst formula and thus to promote the catalyst performance. Of greater importance, the learning gained from the studies of supported Au catalysts may provide reference to the design and development of other noble metal catalysts. For example, by noticing the important roles of ferrihydrite- and ferrihydrite-derived FeO_x supports in the high activity of supported Au catalysts for CO oxidation or CO preferential oxidation in H_2 (PROX),[13−17] a series of ferrihydrite- and FeO_x-supported metal catalysts (Pt, Pd, Ir, Cu) with similar or even better performance have already been developed.[18−24] A recent program entitled “After the Goldrush”—which aims to design and develop catalytic materials by exploiting the learning gained from gold catalysis—suggests clearly that the reference role of study on gold catalysts has been realized.[25]

The CO oxidation on supported gold NPs/clusters therefore has been a paradigm in the last two decades.[26,27] Besides its great importance in practical applications[19,28−30] and the fact that supported Au catalysts are most active for this reaction, a more important reason is that CO oxidation is an ideal model reaction to fundamentally investigate the heterogeneous catalytic mechanism and study the nature of the catalyst.[27] The reaction and product molecules are simple, and no side reaction occurs. However, the most critical issue for oxidation reaction on supported Au catalysts, how to activate the O_2, was involved. Therefore, to effectively address the CO oxidation mechanism on supported Au catalyst may provide guidance/reference to other oxidation reactions on supported Au and even other metal catalysts.

Received: August 6, 2014
Revised: April 30, 2015
Published: April 30, 2015

DOI: 10.1021/cs5020496
ACS Catal. 2015, 5, 3528−3539

Recently, increasing evidence shows that CO oxidation followed, at least partially, the Mars−Van Krevelen (redox) mechanism on reducible-oxides-supported Au catalysts.[31−36] Especially, Li et al. demonstrated that the CO oxidation on the Au/ferrihydrite catalyst was mainly according to a redox mechanism, even at temperatures as low as −60 °C.[37] It suggested that the very high activity of Au/ferrihydrite catalyst actually originated from the high redox property of the ferrihydrite support. Furthermore, this mechanism works for other ferrihydrite-supported noble metals such as Pd and Pt. This finding may provide a new avenue to fabricate highly active supported Au catalysts by using iron oxides/hydroxides with higher redox property. Maghemite (γ-Fe_2O_3) is one of the most common iron oxide polymorphs and has the reverse spinel structure similar to magnetite (Fe_3O_4).[38] Therefore, the reduction of γ-Fe_2O_3 is just related to the loss of O but does not involve any lattice rearrangement. Our current understanding is that despite the similar reducibility of γ-Fe_2O_3 and hematite (α-Fe_2O_3) support, the Au/γ-Fe_2O_3 catalyst was much more reducible than the Au/α-Fe_2O_3 catalyst,[39] which implied a potential higher activity of Au/γ-Fe_2O_3 for CO oxidation according to the redox mechanism.[37]

In this work, we used commercial γ-Fe_2O_3 as a support to develop an exceptionally active Au/γ-Fe_2O_3 catalyst by a facile deposition−precipitation method. By using commercial α-Fe_2O_3 for comparison and through a systemic study, we demonstrated that γ-Fe_2O_3 is a highly active support for a number of metals (Au, Pt, Rh, etc.) for CO oxidation and other reactions that follow a redox mechanism. More importantly, it may provide a feasible avenue to design and develop supported metal catalysts by choosing a suitable crystal phase of the oxide supports.

■ EXPERIMENTAL SECTION

Catalyst Preparation. The commercial nanosphere iron oxides (α-Fe_2O_3 and γ-Fe_2O_3) were purchased from Aladdin Reagent Company and employed directly as supports without any pretreatment.

Gold NPs were deposited onto α-Fe_2O_3 and γ-Fe_2O_3 oxides via a deposition−precipitation process targeting at a gold loading of 5.0 wt %, which was denoted as Au/α-Fe_2O_3 and Au/γ-Fe_2O_3, respectively. For a detailed procedure, see our previous reports.[40,41] For investigating the effect of heat treatment, the two catalysts were further calcined at 300 °C under N_2 atmosphere for 3 h, denoted as Au/α-Fe_2O_3−C and Au/γ-Fe_2O_3−C, respectively.

Other α-Fe_2O_3- and γ-Fe_2O_3-supported noble metal (Pt and Rh) catalysts were also prepared with the same procedure and denoted as M/α-Fe_2O_3−C and M/γ-Fe_2O_3−C (M = Pt and Rh), respectively.

Sample Characterization. The actual metal loadings (Au, Pt, Rh) of various catalysts were determined by inductively coupled plasma atomic emission spectrometer (ICP-AES) on an IRIS Intrepid II XSP instrument (Thermo Electron Corporation).

Brunauer−Emmett−Teller (BET) surface areas of samples were measured by nitrogen adsorption at −196 °C using a Micromeritics ASAP 2010 apparatus. Prior to the measurements, the samples were outgassed at 110 °C to 0.03 Torr for the calcined samples or outgassed at ambient temperature for the uncalcined samples for 12 h to ensure no or little change of the structure of the sample.

The surface composition and the binding energy (B.E.) of the catalysts were determined by X-ray photoelectron spectra (XPS) on an ESCALAB250 X-ray photoelectron spectrometer with contaminated C as the internal standard (C1s = 284.5 eV).

X-ray diffraction (XRD) patterns were recorded on a PW3040/60 X' Pert PRO (PANalytical) diffractometer equipped with a Cu Kα radiation source (λ = 0.15432 nm), operating at 40 kV and 40 mA. A continuous mode was used for collecting data in the 2θ range from 20° to 80° at a scanning speed of 5° min^{-1}.

Room-temperature ^{57}Fe Mössbauer spectra were recorded by using a Topologic 500A spectrometer and a proportional counter. ^{57}Co(Rh) moving with a constant acceleration mode was used as the γ-ray radioactive source. The velocity was calibrated by a standard α-iron foil. The spectra were fitted with the appropriate superpositions of Lorentzian lines using the MossWinn 3.0i computer program. In this way, the ^{57}Fe Mössbauer spectral parameters could be determined, including the isomer shift (IS), the electric quadrupole splitting (QS), effective magnetic field (H), the full width at half-maximum (fwhm), and the relative resonance areas of the different components of the absorption patterns.

Transmission electron microscope (TEM) analyses were performed with a JEOL JEM-2000EM microscope operated at 120 kV. The samples were suspended in ethanol with an ultrasonic dispersion for 5−10 min, and then a few droplets of the suspension were put on a microgrid carbon polymer supported on a copper grid and allowed to dry at room temperature for TEM observations.

Temperature-programmed reduction with CO (CO-TPR) was performed in a quartz microreactor. The samples were purged under He flow at −75 or 25 °C for 15 min. Subsequently, the gas flow was switched to a flow of 5% CO/He (30 mL min^{-1}), and the sample was heated to 900 °C at a rate of 10 °C min^{-1}.

In situ diffuse reflectance infrared Fourier transform (DRIFT) spectra were acquired with a BRUKER Equinox 55 spectrometer equipped with a MCT detector and operated at a resolution of 4 cm^{-1}. All spectra were obtained at room temperature. Before the experiment, the sample (40 mg) in a powder form was purged for 30 min with He at 60 °C. After the samples were cooled to room temperature, the background spectrum was recorded, and then the 1 vol % CO + 1 vol % O_2 balanced with He were introduced into the reaction cell at a total flow rate of 66.7 mL min^{-1} (space velocity, SV = 100 000 mL h^{-1} g_{cat}^{-1}).

In situ Raman spectra were collected using an in situ Raman reactor (Linkam CCR1000) on a LabRam HR800 confocal microprobe Raman instrument (HORIBA Jobin Yvon, France) with laser excitation at 633 nm (He−Ne laser) at a laser power of ca. 0.1 mW. The spectra were obtained by exposure to air and then switching to 10% CO/He at room temperature.

The pulse reactions of CO oxidation on various catalysts were measured with a HT-1000 calorimeter (Setaram, France) which is connected to a pulse reactor system; for details of this apparatus, see previous studies.[37,42] Typically, prior to measurements, 20 mg of sample was purged in flowing He gas at room temperature for 30 min, cooled to −20 °C, and then pulses of the CO and O_2 (0.5 mL) were sequentially admitted to the sample at an interval of 30 min at −20 °C and other temperatures. The effluents were analyzed online by a gas chromatograph (GC, Agilent 6890N). Co-pulse of CO + O_2

Table 1. Physicochemical Properties and Catalytic Activities of Fe_2O_3 and Au/Fe_2O_3 Catalysts

sample	surface area ($m^2\ g^{-1}$)	Au loading (wt %)	D_{Au}[a] (nm)	B.E. of $Au4f_{7/2}$ (eV)	Au^{x+}/Au^{o}	specific rate[b] ($mol_{CO}\ h^{-1}\ g_{Au}^{-1}$)	TOF (s^{-1})	
α-Fe_2O_3	49	--	--	--	--	--	--	this work
Au/α-Fe_2O_3	46	2.9	U.D.[c]	85.0, 86.3	50/50	2.12	0.13[d]	this work
Au/α-Fe_2O_3–C	44	2.9	2.8	84.4	0/100	0.40	0.068[e]	this work
γ-Fe_2O_3	92	--	--	--	--	--	--	this work
Au/γ-Fe_2O_3	84	2.9	U.D.	84.3, 85.6	53/47	33.3	2.02[d]	this work
Au/γ-Fe_2O_3–C	78	2.9	1.9	83.8	0/100	9.85	1.14[e]	this work
Au/Fe_2O_3-WGC	--	4.4	3–4	--	--	0.185	0.045	ref 40
Au/FeO_x	--	3.7	U.D.[c]			3.78	0.23	ref 40
Au/FeO_x	--	1.0	2–3	--	--	3.6–7.3[f]	0.5–1	ref 47
Au/FeO_x	--	2.9[g]	∼0.5	--	--		3.5[h]	ref 56
Au/FeO_x	--	2.9[g]	--	--	--		0.027[i]	ref 56
Au/Fe_2O_3	109	1.0	7.4	--	--	0.94	--	ref 60

[a] Measured by TEM. [b] Measured at 24 °C. [c] Undetected. [d] Using a dispersion of 90%. [e] The gold dispersion was calculated according to $D = 0.9/d_{Au}$, where d means diameter. [f] Calculated from the TOF data by assuming a dispersion of 40%. [g] Atomic percent. [h] TOF of bilayer Au cluster. [i] TOF value of the whole catalyst (i.e., the average of the gold atoms, clusters, and NPs).

was performed with the same procedure, except in each pulse the CO or O_2 was replaced with 0.5 mL of CO + 0.5 mL of O_2.

Catalytic Performance Test. The catalytic activity for CO oxidation was measured using a continuous-flow fixed-bed reactor system. For each test, 50 mg of the catalyst sample powder diluted with about 350 mg of SiO_2 was loaded into a U-shape quartz reactor. After being purged with He for 30 min at room temperature, a feed stream containing 1 vol % CO and 1 vol % O_2 balanced with He was allowed to pass through the catalyst sample at a flow rate of 66.7 mL min^{-1}, resulting in a space velocity (SV) of 80 000 mL $g_{cat}^{-1}\ h^{-1}$. The inlet and outlet gas compositions were analyzed by an online gas chromatograph with TCD detector using helium as carrier gas (HP 6890, TDX-01 column).

The activity for water gas shift (WGS) reaction was measured in the same procedure except that the reaction gas composition was 2 vol % CO + 10 vol % H_2O balanced with He.

The specific rates were measured under a differential model where the CO conversions were controlled below 25%. The conversions of CO during the first 60 min were averaged and used for calculations of the specific reaction rates.

RESULTS

Catalyst Structure and Surface Property. Some physicochemical properties of the iron-oxides- and Au-supported catalysts are presented in Table 1. It shows that the surface areas of both iron oxides are small (<100 $m^2\ g^{-1}$), although the surface area of γ-Fe_2O_3 is higher than that of α-Fe_2O_3. After loading of Au, the surface areas of both oxides decreased slightly, suggesting that some of the pores or the adsorption sites were occupied by the gold species. The actual Au loadings on both iron oxides are 2.9 wt %, much lower than the nominal value. This might be due to the loss of Au during the deposited process.[40,43,44]

Figure 1 shows the XRD patterns of the iron oxides and the iron-oxides-supported Au catalysts. Both oxides presented their typical diffraction patterns, suggesting the pure phase of the iron oxides. After loading of Au, neither the crystal phase nor the nanoparticle size of α-Fe_2O_3 and γ-Fe_2O_3 oxides changes. Because γ-Fe_2O_3 has the same XRD patterns with that of Fe_3O_4 and because γ-Fe_2O_3 tends to transform to α-Fe_2O_3 under calcination at elevated temperature, we further performed ^{57}Fe Mössbauer measurements to confirm the γ-Fe_2O_3 phase before and after calcination. From Figure 2 and the corresponding fitting analysis (Table S1), we can confirm the as-received γ-Fe_2O_3 phase and claim that there is no phase transformation for the Au/γ-Fe_2O_3–C catalyst after being calcined at 300 °C under N_2 atmosphere. In addition, no diffraction peaks of Au or Au oxides were observed on all α-Fe_2O_3 and γ-Fe_2O_3-supported Au catalysts, suggesting that the Au was highly dispersed on the iron oxides, even after being calcined at 300 °C.

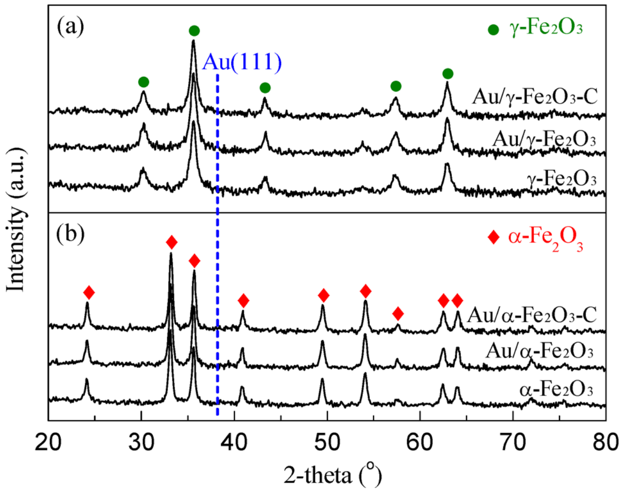

Figure 1. XRD patterns of (a) γ-Fe_2O_3, Au/γ-Fe_2O_3 and Au/γ-Fe_2O_3–C and (b) α-Fe_2O_3, Au/α-Fe_2O_3 and Au/α-Fe_2O_3–C.

The size of the Au NPs has been regarded as one of the most important factors to determine their catalytic activity.[7,45,46] To measure the size of the gold NPs, we examined the catalysts with TEM. The typical images and the size distribution of Au NPs are presented in Figure 3. It shows that no Au NPs could be observed on the Au/α-Fe_2O_3 and Au/γ-Fe_2O_3 catalysts, Figure 3a,b, suggesting that the Au species were highly dispersed on both iron oxides as clusters smaller than 1 nm that cannot be detected by the TEM.[14,17,40] After calcination at 300 °C, visible Au NPs with size of 1−4 nm are clearly observed on both catalysts, Figure 3c,d, suggesting that the Au clusters aggregated during calcination. The size distributions, Figure 3e,f, show that the Au NPs on Au/γ-Fe_2O_3–C were slightly smaller than that on Au/α-Fe_2O_3–C (mean diameter of

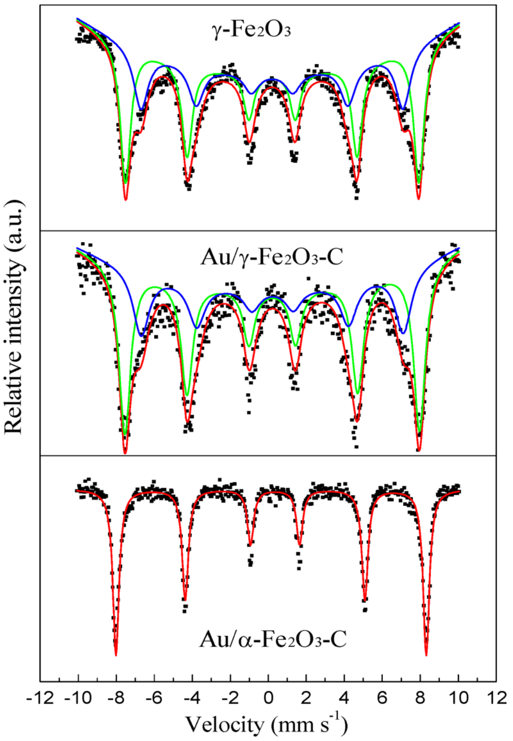

Figure 2. Room-temperature ^{57}Fe Mössbauer spectra of as-received γ-Fe_2O_3, Au/γ-Fe_2O_3−C and Au/α-Fe_2O_3−C.

1.9 nm vs 2.8 nm), indicating that the degree of aggregation was slightly different. This suggests that the interaction between Au and γ-Fe_2O_3 might be stronger than that between Au and α-Fe_2O_3. However, despite the slight difference in Au NP size, these values are both in the optimize size of <5 nm for a highly active Au catalyst.[7,47] Therefore, the size effect on the two types of oxides-supported catalysts, regardless of calciation or not, could be to a large extent excluded.

The chemical valence of the Au species is another important factor that affect their CO oxidation activity dramatically.[48] The measurements of Au4f XPS spectra were therefore performed. As shown in Figure S1 and Table 1, the Au species on Au/γ-Fe_2O_3 and Au/α-Fe_2O_3 catalysts are a mixture of Au^0 and Au^{x+} without calcination treatment, in line with the previous iron-oxides-supported Au catalysts.[17,40] A quantitative analysis shows that the ratios of Au^{x+}/Au^0 were about 1 for both samples, suggesting that without calcination treatment the chemical states of Au species on both samples are similar. After being calcined at 300 °C, as expected, the Au oxides/hydroxides decomposed completely on both iron oxides, also in line with the previous reports.[17,40] This indicated that with or without calcination the chemical states of Au are similar on both iron oxides. The chemical state effect of Au species thus could be ruled out as well. It should be noted that the B.E. of Au4f for α-Fe_2O_3-supported catalysts is slightly higher than that of γ-Fe_2O_3-supported ones. This should be due to the support charging effect which arouse the shifting of the peak position and the broadening of the peak width.[49] It was reported that the B.E. shift of Au is size- and support-dependent: An increased (positive) B.E. shift correlated with the decreasing of the Au cluster size and the support conductivity.[50] Although α-Fe_2O_3 and γ-Fe_2O_3 are both semiconductors, the band gap of α-Fe_2O_3 is higher than that of γ-Fe_2O_3, suggesting its conductivity is lower.[51] Therefore, the B.E. of Au supported on α-Fe_2O_3 should be higher than that on γ-Fe_2O_3. Furthermore, the Au4f peak for Au/α-Fe_2O_3−C is obviously wider than that for Au/γ-Fe_2O_3−C, also indicating a higher charging effect on Au/α-Fe_2O_3−C than on Au/γ-Fe_2O_3−C sample. It also shows that the uncalcined sample have higher Au4f B.E. than their calcined counterparts. This should be due to the size effect[50,52] because the size of the Au clusters on uncalcined samples are much smaller than that on the calcined ones.

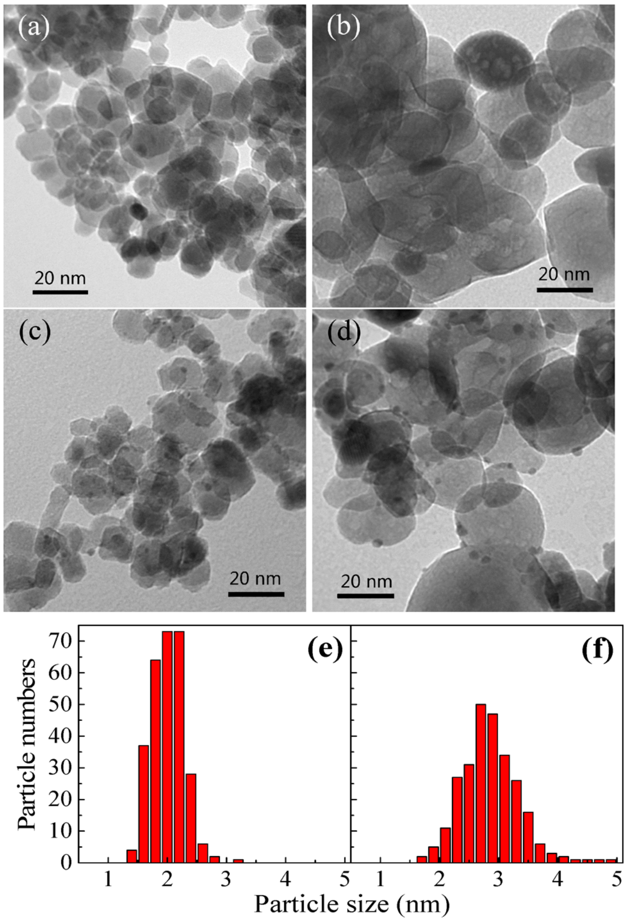

Figure 3. Typical TEM images of Au/γ-Fe_2O_3 (a), Au/α-Fe_2O_3 (b), Au/γ-Fe_2O_3−C (c), and Au/α-Fe_2O_3−C (d) and size distribution of Au NPs on Au/γ-Fe_2O_3−C (e) and Au/α-Fe_2O_3−C (f).

It has been reported that surface OH^- group had a great influence on the activity of CO oxidation on the supported Au catalyst.[53−55] The XPS spectra of O1s for the four samples were also measured and analyzed in detail. As shown in Figure S2, the O1s XPS spectra exhibited a broadened peak, including a main peak centered at ~530 eV and a shoulder peak centered at ~532 eV. After fitting analysis, as shown in Table 2, the O species were composed of lattice O (~530 eV), OH^- group (~531.5 eV)[56−58] and adsorbed H_2O (~533.0 eV).[59] The ratios of these three species in all catalysts are 72−75% for lattice O, 20−24% for OH^- group O and ~5% for adsorption H_2O. Clearly, the amount of OH^- group species in all the catalysts were similar. Therefore, the effect of OH^- group could also be ruled out.

Catalyst Activity. The samples were tested for CO oxidation with a gas composition of 1 vol % CO + 1 vol % O_2 + He, Figure 4. It shows that both α-Fe_2O_3 and γ-Fe_2O_3 are inactive for CO oxidation at temperature below 150 °C. At a

Table 2. Oxygen Species in the Two Iron Oxides Supported Au Catalysts Obtained from the O1s XPS Analysis

sample	B.E. (eV)	O species	percent (%)
Au/γ-Fe_2O_3	529.9	lattice O	72
	531.5	OH^-	24
	533.0	H_2O	4
Au/γ-Fe_2O_3-used	530.1	lattice O	73
	531.5	OH^-	21
	533.1	H_2O	6
Au/γ-Fe_2O_3−C	530.0	lattice O	76
	531.6	OH^-	20
	532.9	H_2O	4
Au/γ-Fe_2O_3−C-used	529.9	lattice O	78
	531.2	OH^-	17
	533.1	H_2O	5
Au/α-Fe_2O_3	529.8	lattice O	74
	531.3	OH^-	21
	533.1	H_2O	5
Au/α-Fe_2O_3−C	529.7	lattice O	72
	531.5	OH^-	22
	532.8	H_2O	6

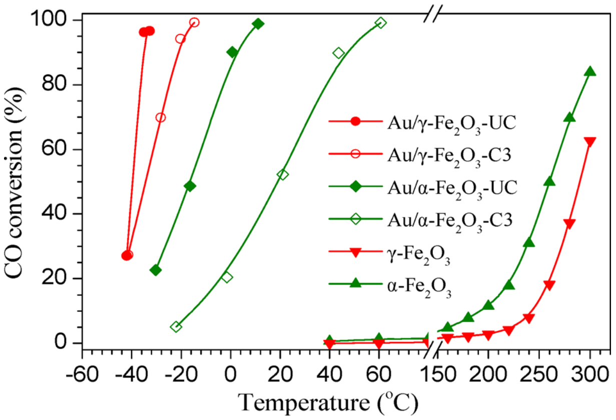

Figure 4. CO conversion as a function of reaction temperature on different Au/Fe_2O_3 catalysts for CO oxidation. One vol % CO + 1 vol % O_2 + 98 vol % He, SV = 80 000 mL g_{cat}^{-1} h^{-1}.

temperature range of 150−300 °C, α-Fe_2O_3 exhibits higher activity than that of γ-Fe_2O_3. After Au was loaded, the catalytic activities increase dramatically, suggesting that the Au or the entities of Au/iron oxides are much more active than iron oxides themselves. However, the degrees of activity increase are significantly different. In contrary to the activity order of the bare iron oxides, γ-Fe_2O_3-supported Au catalysts exhibit much higher activity than that of α-Fe_2O_3-supported Au catalysts: Au/γ-Fe_2O_3 and Au/γ-Fe_2O_3−C can totally oxidize CO at temperature lower than or around −20 °C; the Au/α-Fe_2O_3 and Au/α-Fe_2O_3−C catalysts, however, can only completely oxidize CO at 10 and 60 °C, respectively.

To obtain the intrinsic activity of these catalysts for a more accurate comparison and to compare with the catalysts reported in literatures,[60] we measured their specific reaction rates for CO oxidation at 24 °C and calculated the corresponding TOF values, Table 1. The activity comparison can be based on either the initial activities or the steady-state activities. Here we'd like to measure their initial specific rate for comparison, although the reaction stabilities of all the catalysts are good (stability tests are shown below). However, to avoid the probably occasional abnormal or inaccurate data obtained in one time, we used the average activity at 20, 40, and 60 min. We also compared the activity at 20 min and the average activity at 20, 40, and 60 min, Figure S3, Table S2. Although the activity at 20 min is slightly higher than that of the average of 60 min, they are indeed very similar, suggesting that the activity did not change much during the first 1 h. As shown in Table 1, the Au/α-Fe_2O_3 and Au/α-Fe_2O_3−C catalysts exhibit similar or higher TOFs compared with the standard Au/Fe_2O_3−WGC catalyst (entry 7, Table 1) and higher specific rates. Especially, the Au/α-Fe_2O_3 yields a specific rate of 2.12 mol_{co} g_{Au}^{-1} h^{-1} (corresponding to ∼0.06 mol_{co} g_{cat}^{-1} h^{-1}), suggesting it possessed high activity according to Schuth's definition (0.02 mol_{co} g_{cat}^{-1} h^{-1}).[61] Compared with α-Fe_2O_3-supported Au catalysts, the γ-Fe_2O_3-supported Au catalyst exhibits much higher activity: it yields TOFs of 2.02 and 1.14 s^{-1} for Au/γ-Fe_2O_3 and Au/γ-Fe_2O_3−C, respectively, which was about 15−20 times higher than that of Au/α-Fe_2O_3 and Au/α-Fe_2O_3−C catalysts. They are even more active than 2−3 nm Au colloidal on FeO_x, which is one of the most active Au catalysts (entry 9, Table 1).[47] The highly active Au species in the optimized size range of 0.5−5 nm usually generate the TOF of around 1 s^{-1}.[61,62] Therefore, our γ-Fe_2O_3-supported Au catalysts are among the most active supported Au catalysts. Because the TOF of Au/γ-Fe_2O_3 catalyst was obtained by using a 90% dispersion, their specific rate is particularly high, reaching to 33.3 mol_{co} g_{Au}^{-1} h^{-1} (corresponding to 1 mol_{co} g_{cat}^{-1} h^{-1}, about 50 times higher than the highly active Au catalyst[61]). In fact, to our best knowledge, it is the most active catalyst at room temperature reported so far. Chen et al. have reported a bilayer structure of Au species possessed a TOF of 4 s^{-1}.[63] However, their data were obtained from model catalyst. Herzing et al. subsequently reported a similar data of ∼3.5 s^{-1} of the bilayer structure in a real catalyst of Au/FeO_x (entry 10, Table 1),[56] while the fraction of this bilayer structure in all Au species was only 0.6 atom %, which resulted in a much lower activity of the whole catalyst (0.027 s^{-1}, entry 11, Table 1).

Correlation of Activity and Redox Property of the Catalysts. It was reported that the iron-oxides-supported Au catalysts were mainly according to a redox mechanism at low temperature, and the high activity of Au/ferrihydrite catalysts originated from its high redox property.[37] To demonstrate that this redox mechanism is general for iron-oxides-supported Au catalysts and to correlate the redox property with activity, we measured the reducibility of these α-Fe_2O_3 and γ-Fe_2O_3-supported catalysts with CO-TPR, Figure 5. Prior to the catalyst measurements, the bare iron oxides of α-Fe_2O_3 and γ-Fe_2O_3 were first measured as reference for comparison. As shown in Figure 5a, both α-Fe_2O_3 and γ-Fe_2O_3 exhibit one sharp peak at 250−300 °C and a broad band at temperature >350 °C, which correspond to the reduction of α-Fe_2O_3/γ-Fe_2O_3 to Fe_3O_4 and further to FeO/Fe species, respectively.[64,65] The temperature of the sharp peak for α-Fe_2O_3 is lower than that for γ-Fe_2O_3, suggesting that α-Fe_2O_3 is easier to be reduced with CO to form Fe_3O_4. This is in line with the activity test result that α-Fe_2O_3 is more active than γ-Fe_2O_3. However, after introduction of Au species, the reduction behavior of the catalysts changed. For Au/α-Fe_2O_3 and Au/γ-Fe_2O_3 catalysts, there are two sharp reduction peaks and a broad reduction band. The first peak (denoted as peak I) centered at about −5 °C can be ascribed to the reduction of Au^{x+} species. The second peak (denoted as peak II) corresponds to the reduction of α-Fe_2O_3/γ-Fe_2O_3 to Fe_3O_4.

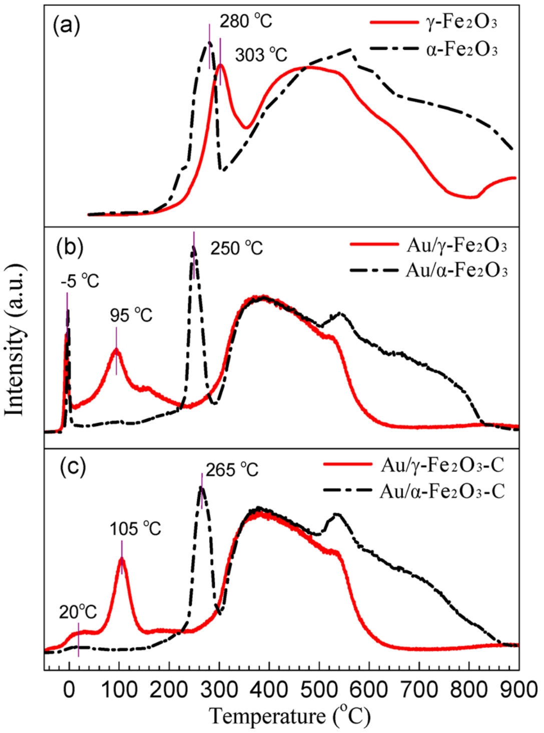

Figure 5. CO-TPR profiles of (a) α-Fe_2O_3 and γ-Fe_2O_3, (b) Au/α-Fe_2O_3 and Au/γ-Fe_2O_3, and (c) Au/α-Fe_2O_3−C and Au/γ-Fe_2O_3−C.

Compared with the bare iron oxides, the reduction temperatures of peak II for both catalysts decrease, suggesting that the presence of Au promoted the reduction of iron oxides. However, the decrease extent varies significantly: for Au/α-Fe_2O_3, it decreased slightly from 280 to 250 °C, while for Au/γ-Fe_2O_3, it decreased dramatically from 300 °C to only 95 °C. This result indicates clearly that although the reducibility of γ-Fe_2O_3 is slightly lower than that of α-Fe_2O_3, it becomes much higher after it was collaborated with Au species. The different promoting effect is probably due to the different interaction between Au and the iron oxides, which will be discussed later. As to the Au/α-Fe_2O_3−C and Au/γ-Fe_2O_3−C catalysts, their reduction behaviors are similar to that of the Au/α-Fe_2O_3 and Au/γ-Fe_2O_3, except that the sharp peak I disappeared. This is as expected because the XPS data proved that the Au^{x+} species was reduced after calcination at 300°, Table 1. However, there is still a visible broad band from −20 to 60 °C on Au/γ-Fe_2O_3−C catalysts (Figure S4), which proved that some lattice oxygen, most probable the surface O that closely contacted with Au species, can be reduced by CO at temperature as low as ca. −20 °C. The area ratio of this band to peak II was calculated to be about 1:7, showing that the percentage of these O species is about 14%. In the case of Au/α-Fe_2O_3−C, however, this band is ambiguous and the area ratio to peak II is about 1:25, suggesting a much lower percentage of reactive lattice O species.

The CO-TPR results show clearly that the reducibility of iron oxides and the catalysts are well consistent with their activity for CO oxidation. To further corroborate that the high activity of γ-Fe_2O_3-supported catalysts actually originated from their high redox properties, the pulse reactions of CO oxidation were further performed at −20 °C where the activity of CO oxidation on α-Fe_2O_3- and γ-Fe_2O_3-supported Au catalysts had distinct differences according to Figure 4. This method is effective to verify the redox mechanism.[37] Figure 6 illustrates the consumption of CO and O_2 as well as the production of CO_2 on various catalysts. As shown in Figure 6a,b, it consumes about 200 and 160 μmol g_{cat}^{-1} CO and meanwhile produced about 120 and 100 μmol g_{cat}^{-1} CO_2 with each pulse of CO on Au/γ-Fe_2O_3 and Au/γ-Fe_2O_3−C catalysts, respectively. In each O_2 pulse, the consumption of O_2 was about half that of CO or less under steady state without producing CO_2. This clearly suggested that the CO oxidation accomplished in the CO pulse process by reacting with the surface/subsurface lattice O of the γ-Fe_2O_3 support, while the O_2 replenished the consumed lattice O in the O_2 pulse process, demonstrating the redox mechanism of CO oxidation. The amount of CO_2 production in each pulse was lower than that of the CO consumption because part of the produced CO_2 was absorbed on the oxide support to form carbonates.[37] The nonstoichiometric consumption of O_2 may be due to that the adsorption and accumulation of CO_2 occupies some of the adsorption sites. Similarly, on the Au/α-Fe_2O_3 catalyst (Figure 6c), the same phenomenon is observed with the sequential pulses of CO and O_2 except that the amounts of CO consumption and CO_2 production are much lower than that on Au/γ-Fe_2O_3 and Au/γ-Fe_2O_3−C catalysts, in line with the activity results. Furthermore, the amounts of CO consumption and CO_2 production increase with the reaction temperature, indicating that the redox process is more favorable at elevated temperatures. As to the Au/α-Fe_2O_3−C catalyst (Figure 6d), there is no CO_2 production in both CO and O_2 pulses, which is well consistent with the fact that this catalyst is inactive for CO oxidation at −20 °C

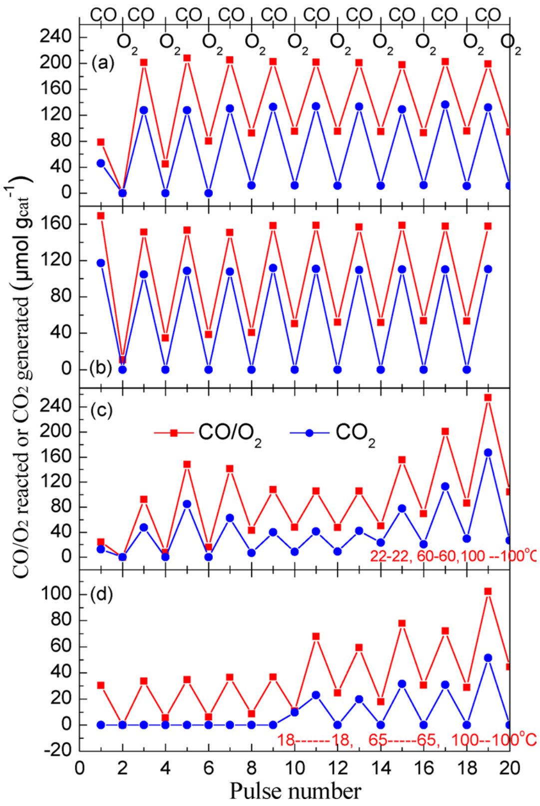

Figure 6. Sequential pulses of CO and O_2 (square symbol) and generation of CO_2 (circle symbol) on (a) Au/γ-Fe_2O_3, (b) Au/γ-Fe_2O_3−C at −20 °C, (c) Au/α-Fe_2O_3, and (d) Au/α-Fe_2O_3−C at −20, ca. 20, ca. 60, and 100 °C.

(conversion <5%). The redox reaction only occures when reaction temperature increased to ca. 20 °C, and the amounts of CO consumption and CO_2 production also increased with the increase of the reaction temperature.

The above pulse reactions unambiguously demonstrated that CO oxidation could follow a redox mechanism. However, this method could not exclusively prove that CO reacted with the lattice O of the iron oxides (Fe−O species) because a possibility of CO reaction with other O_2-containing species (for example, a possible stably adsorbed O species) could not be thoroughly ruled out. However, the redox reaction with Fe−O species must result to the change of the iron oxides. We therefore employed the Raman spectroscopy, which is a powerful technique to detect the surface change of oxides to confirm the redox reaction between Fe^{3+} and Fe^{2+}. Figure 7 presents the in situ Raman spectra of Au/γ-Fe_2O_3−C and Au/α-Fe_2O_3−C exposed to different atmosphere. For Au/γ-Fe_2O_3−C in air, it exhibits four bands (370, 490, 667, 720 cm^{-1}), which are typical γ-Fe_2O_3 features.[66] It should be particularly noted that the 720 cm^{-1} band were attributed to the vibrational modes of local Fe−O structures in the vicinity of cation vacancies.[67] When the air flow is replaced with 10 vol % CO/He, the 720 cm^{-1} band disappears first, suggesting that the O species located at the cation vacancies were most activated and had the highest activity. Then other bands disappear gradually with time evaluation, and only the band at 667 cm^{-1} remains. The 667 cm^{-1} band is the typical feature of Fe_3O_4, suggesting that the surface Fe^{3+} has been partially reduced into Fe^{2+} under CO atmosphere to form Fe_3O_4.[66,68] When the gas flow is switched from 10 vol % CO/He to air, the feature bands of γ-Fe_2O_3 appear again, indicating that surface Fe^{2+} is reoxidized to Fe^{3+} under air flow. The in situ Raman spectra apparently demonstrate the redox process of $Fe^{3+}\leftrightarrow Fe^{2+}$ existed on the surface of Au/γ-Fe_2O_3−C catalyst. On the contrary, for the Au/α-Fe_2O_3−C catalyst, it shows the typical α-Fe_2O_3 feature bands in both air and 10 vol % CO/He gas flow, suggesting that no redox reaction occurred or the reaction was too weak to be detected at room temperature.

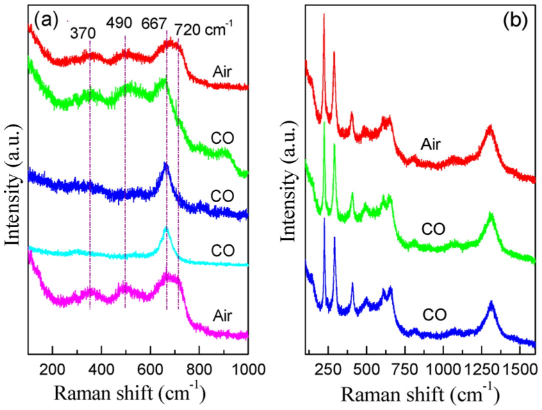

Figure 7. In situ Raman spectra of (a) Au/γ-Fe_2O_3−C and (b) Au/α-Fe_2O_3−C obtained in different atmosphere at room temperature.

Comparison of Sequential Pulse and Copulse of CO and O_2 Reaction. To roughly estimate the percentage of the redox pathway in the overall reaction, we further compared the CO consumption and CO_2 generation in sequential pulse of CO and O_2 and copulse of CO + O_2 reaction.[37] As shown in Figure S5a, for the Au/γ-Fe_2O_3 catalyst at steady state, it consumes about 210 μmol g_{cat}^{-1} CO in each CO pulse in sequential pulse reaction, while it consumes about 380 μmol g_{cat}^{-1} in each CO + O_2 pulse. Meanwhile, it separately generates about 130 and 360 μmol g_{cat}^{-1} CO_2. The much lower CO_2 yields (denoted as percentage of CO_2 generation to CO consumption) in sequential pulse process (~62% vs ~95%) suggests that CO_2 adsorption and accumulation is much more serious than that during the copulse process which is general for all the samples (Figure S5). From the CO consumption ratio of sequential pulse to copulse process, we can roughly estimate that the redox process accounts for at least 55% in the overall reaction.[37] Considering that the CO_2 accumulation in sequential pulse reaction may hinder the subsequent O adsorption and reaction and that in the copulse process the O_2 species can be replenished timely, thus each active site may participate in the reaction more than once during a single pulse, it is reasonable to conjecture that the redox process might take an even higher percentage. Similarly, for Au/γ-Fe_2O_3−C, the redox process accounts for about 50% percent. For Au/α-Fe_2O_3 and Au/α-Fe_2O_3−C catalyst, the redox process also account for about 50% or even higher at −20 °C. However, at elevated temperatures, the percentages decrease significantly, suggesting that the dominating reaction mechanism changes at higher temperature, especially for Au/α-Fe_2O_3−C catalyst. This also explains the above result that no redox process was detected in in situ Raman measurement (Figure 7) while there was high CO conversion (~50%, Figure 4) for Au/α-Fe_2O_3−C catalyst at 20 °C.

Catalyst Stabilities and Characterizations of Used Samples. It should be mentioned that all the reaction data were tested for initial activity, and the characterization was performed for the fresh sample. One may argue whether the activity comparison is still valid at their steady state and wonder whether the characterizations are representative. In addition, the stability of a catalyst is a crucial factor for its catalytic application. This is particularly true for the supported Au catalysts since their reaction stabilities are usually low and the stability issue has been a major barrier to their practical application.[69] Therefore, we further tested the stabilities of these Au catalysts by significantly increasing the SV to avoid the activity saturation. As shown in Figure 8, all samples show good reaction stability: the CO conversions drop only 10−20% during the 100 h test. Of more importance, the γ-Fe_2O_3-supported catalysts show similar or even better stability compared to the α-Fe_2O_3-supported ones, demonstrating that they are certainly more active, either for initial activity or in their steady state. The good stabilities make them more

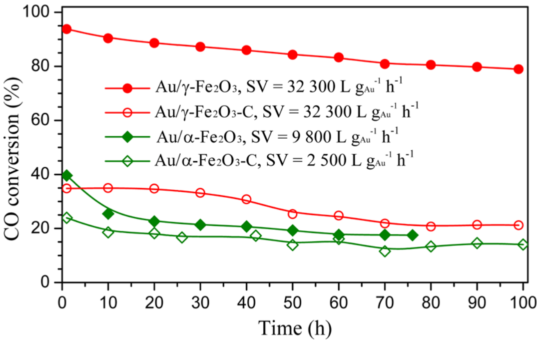

Figure 8. CO oxidation stabilities of various Au/Fe_2O_3 catalysts at 30 °C.

applicable. The samples after stability test were examined by TEM and XPS to characterize the possible changes in size and oxidation state of Au. Figure S6 presents the TEM images of various fresh and used samples and their corresponding Au particle size distribution. For Au/α-Fe_2O_3 and Au/γ-Fe_2O_3 catalysts, some ambiguous Au NPs could be observed after the 100 h test, suggesting that sintering of Au species occurred during reaction, which may mainly account for the rapid initial deactivation. Comparatively, there are no significant size changes on Au/α-Fe_2O_3−C and Au/γ-Fe_2O_3−C because they were preheated at 300 °C. The Au4f XPS (Figure S7) show that after the 100 h test, Au species on all samples are Au^0. This suggests that Au^{x+} species on Au/α-Fe_2O_3 and Au/γ-Fe_2O_3 catalysts were reduced during reaction, which is consistent with previous studies.[37,70] The O1s XPS were also measured (Figure S8) and fitted (Table 2). Clearly for Au/γ-Fe_2O_3 and Au/γ-Fe_2O_3−C catalyst, there is no detectable O specie change. For Au/α-Fe_2O_3 and Au/α-Fe_2O_3−C catalysts, unfortunately, the diluent SiO_2 contributed to the O spectra (γ-Fe_2O_3-supported catalysts can be purified by magnetic separation), so the fitting analysis is not available. However, based on the results of γ-Fe_2O_3-supported catalysts, it is reasonable to conjecture that there's no significant change of O species on α-Fe_2O_3-supported Au catalysts either.

To detect the change of oxidation state of Au species, we further performed in situ DRIFT spectroscopy measurements of different Au catalysts under CO oxidation reaction. As shown in Figure S9a,b, on Au/γ-Fe_2O_3 and Au/α-Fe_2O_3 catalysts, three CO adsorption bands centered at 2180, 2160, and 2110 cm^{-1} are observed, which could be attributed to gas CO, CO adsorption on Au^+ and Au^0 species,[71] respectively. It shows clearly that the Au^+ species are rapidly reduced to Au^0 within 2 min. Comparatively, on Au/γ-Fe_2O_3−C and Au/α-Fe_2O_3−C catalysts, there are only two bands at 2180 and 2110 cm^{-1} (Figure S9c,d), suggesting that the Au species existed as Au^0 at the beginning. This is well consistent with the XPS results. In addition, on all samples obvious adsorption bands at carbonate region (1200−1600 cm^{-1}) are observed, suggesting the adsorption and accumulation of CO_2 occurred during reaction, which is in line with the CO pulse reaction results.

Other Iron-Oxides-Supported Metal Catalysts for CO Oxidation. The above activity and characterization data unambiguously demonstrated the following: (i) the redox mechanism was universal for iron oxides such as γ-Fe_2O_3-supported Au catalysts; (ii) γ-Fe_2O_3-supported Au catalysts had better reducibility and redox property than α-Fe_2O_3-supported ones; (iii) γ-Fe_2O_3-supported Au catalysts, therefore, had higher activity for CO oxidation than α-Fe_2O_3-supported ones. It was reported that the redox mechanism of Au/ferrihydrite for CO oxidation can be extended to other noble metals such as supported Pd, Pt catalysts.[37] Accordingly, we can expect that γ-Fe_2O_3-supported Pt, Pd catalysts would be more active for CO oxidation than α-Fe_2O_3-supported ones. To verify this, we prepared α-Fe_2O_3- and γ-Fe_2O_3-supported Pt and Pd catalysts with the same method and tested their activities for CO oxidations. As shown in Figure 9, as expected, the Pt/γ-Fe_2O_3−C certainly exhibits much higher activity than that of the Pt/α-Fe_2O_3−C at the measurement temperature range. However, it should be noted that the Pt loading on Pt/γ-Fe_2O_3−C is double of that on Pt/α-Fe_2O_3−C (Table 3), although the nominal Pt loadings (5.0 wt %) were same. This indicated that Pt loss also occurred during the prepared process, and the loss extent was different, probably due to the different interaction between Pt and the iron oxides. Therefore, to give a more reasonable comparison, we measured their specific rates for CO oxidation, Table 3. Clearly, the activity of Pt/γ-Fe_2O_3−C is about 8 times higher than that of Pt/α-Fe_2O_3−C in terms of per weight of Pt. The Pd/α-Fe_2O_3−C and Pd/γ-Fe_2O_3−C catalysts were also prepared, but unfortunately, the Pd metal could not be deposited on both iron oxides. The reason is not clear yet and needs to be further studied. We thus chose Rh, another Pt-group metal which has been regarded as a good candidate for CO oxidation,[22,72−74] to prepare Rh/α-Fe_2O_3−C and Rh/γ-Fe_2O_3−C to further verify this trend. As shown in Table 3, although the difference is not as large as that of Pt and Au catalysts, the activity of Rh/γ-Fe_2O_3−C is still 3 times higher than that of the Rh/α-Fe_2O_3−C catalyst. The TOFs were calculated based on a 90% dispersion because the TEM images showed that there were no visible NPs on all samples, Figure S10.

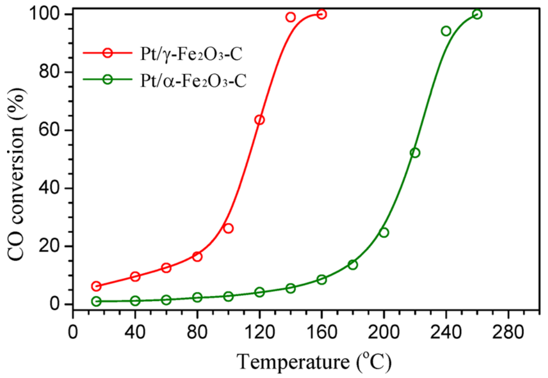

Figure 9. CO conversion as a function of reaction temperature for CO oxidation on 1.3 wt % Pt/γ-Fe_2O_3−C and 0.6 wt % Pt/α-Fe_2O_3−C catalysts. One vol % CO + 1 vol % O_2 + 98 vol % He, SV = 80 000 mL g_{cat}^{-1} h^{-1}.

Table 3. Specific Rates and TOFs of Iron-Oxides-Supported Pt and Rh Catalysts for CO Oxidation at 150 °C

sample	metal loading (wt %)	specific rate (mol_{CO} g_{metal}^{-1} h^{-1})	TOF $\times 10^3$ (s^{-1})
Pt/α-Fe_2O_3−C	0.6	0.24	14.2
Pt/γ-Fe_2O_3−C	1.3	1.91	115.2
Rh/α-Fe_2O_3−C	4.0	0.09	2.6
Rh/γ-Fe_2O_3−C	4.4	0.27	7.8
Au/α-Fe_2O_3[a]	2.9	0.08	5
Au/γ-Fe_2O_3[a]	2.9	0.42	25

[a] For WGS reaction at 120 °C.

To prove that on these catalysts CO oxidation also followed a redox mechanism and positively correlated with their reducibility, we further performed CO-TPR and CO pulse reaction measurements. From Figure S11, we can see that both Pt and Rh promoted the reduction of γ-Fe_2O_3 to Fe_3O_4 significantly (lower than 200 °C), whereas it did not promote, or minimally promoted, the reduction of α-Fe_2O_3. This results are similar to that of the supported Au catalysts. Similarly, the CO pulse reactions (Figure S12) also show that the redox cycles occurred on γ-Fe_2O_3-supported catalysts more than it did on α-Fe_2O_3-supported catalysts, although the difference is different from that of supported Au catalysts.

Activity of Other Reaction with or Following Redox Mechanisms. All experimental data above show very good positive correlation between the redox properties and the activity for CO oxidation due to that CO oxidation is mainly according to the redox mechanism on the iron-oxides-supported catalysts in the measurement temperature range. Therefore, we can further conjecture that for other reactions that follow redox mechanism the γ-Fe_2O_3-supported Au catalysts would also have higher activity than that of α-Fe_2O_3-supported ones. WGS is an old but important industrial processes employed in energy conversion and H_2 gas purification.[75] This reaction has been well accepted to follow a redox mechanism on iron oxides at high temperatures. Recently, a dominant redox (regeneration) mechanism for iron-oxide-supported Au catalysts has also been proposed.[75−78] We therefore chose WGS as a probe reaction to verify this prediction. The results presented in Table 3 clearly show that, although their activities are much lower than that of CO oxidation, the Au/γ-Fe_2O_3 is about 5 times more active than Au/α-Fe_2O_3, suggesting the critical role of the high redox property of γ-Fe_2O_3. However, it should be noted that although the redox mechanism has been well accepted for Au/Fe_2O_3 catalysts,[75−78] a possibility that the redox properties of the support material are crucial in the WGS reaction with an associative mechanism that invokes the formation of stable surface intermediates located at oxygen vacancies cannot be exclusively ruled out. Therefore, a detailed mechanism study is needed.

■ DISCUSSION

It was reported that CO oxidation on ferrihydrite-supported Au catalysts obeyed the redox mechanism.[37] Therefore, the catalyst with higher redox properties would have better activity. However, in that report,[37] all samples were prepared with a coprecipitation method. To compare the ferrihydrite- and α-Fe_2O_3-supported catalysts, the samples were treated at different temperatures (e.g., dried at 60 °C vs calcined at 400 °C). Therefore, some other factors, such as the size of Au NPs, the chemical state of Au species, and surface OH^- groups, which were thought to dramatically affect the activity of supported Au catalysts, varied. In this work, to exclude the effect of these factors, we use commercial iron oxides as supports and deposit the Au NPs by a deposition−precipitation method, which ensured that all Au species were dispersed on the surface of the supports. Furthermore, we made the same heat treatments on both samples (i.e., dried at 60 °C only and calcined at 300 °C under N_2 atmosphere). By taking these procedures, α-Fe_2O_3- and γ-Fe_2O_3-supported Au catalysts, with or without calcination, have similar size of Au NPs (Figure 3), chemical state of Au species (Table 1, Figure S1) and amount of surface OH^- group (Table 2, Figure S2). In this case, we can claim that the effect of these factors has been, at least majorly, ruled out. The activity of CO oxidation can be therefore directly correlated to the redox properties of the catalysts. The subsequent activity test results had very good correlation with the CO-TPR characterization results, as shown in Figure 4 and Figure 5. The surface pulse reaction of CO and O_2 and in situ Raman spectra further confirmed that the high activity of γ-Fe_2O_3-supported Au catalysts originated from their high redox properties, Figure 6 and Figure 7.

It was suggested that the redox mechanism was universal for other ferrihydrite-supported metal (such as Pt and Pd) catalysts.[37] Because we have demonstrated in this work that redox mechanism also works for γ-Fe_2O_3-supported Au catalysts, we can therefore expect that other γ-Fe_2O_3-supported metal catalysts would have higher activity for CO oxidation than that of α-Fe_2O_3-supported ones. The certain examples (Pt and Rh in this work) have further verified the prediction, although their activities and differences in activity varied, Figure 9 and Table 3. Moreover, on the basis of these success predictions, we can further expect that other reactions that follow redox mechanism have the same activity order. As expected, the γ-Fe_2O_3-supported Au catalyst certainly showed higher activity for the selected probe reaction (WGS reaction in this work) than that of α-Fe_2O_3-supported Au catalyst, Table 3.

The study in this work revealed that γ-Fe_2O_3 could be a good support for many metals to prepare highly active catalysts, which was rarely noticed before.[39,79−81] Particularly, the Au/γ-Fe_2O_3 showed exceptionally high activity for CO oxidation and presented the highest activity so far except the bilayer structure of Au in a model catalyst.[63] γ-Fe_2O_3 is one of the most common polymorphs in many iron oxides.[82] Although it is less stable than α-Fe_2O_3, the most stable polymorph among iron oxides, it is much more stable than ferrihydrite. Ferrihydrite is highly reducible, and the metal/ferrihydrite catalyst had very good redox property.[37] Therefore, metal/ferrihydrite entities are highly active for CO oxidation and PROX reaction.[13−22,24,83] Theoretically, they should also have very high activity for other reactions that follow the redox mechanism. However, ferrihydrite is not heat-resistant. Even middle-temperature heat treatment (e.g., 200 °C) may arouse the phase transformation and result in the activity decrease.[15−17,37] This heating nonresistance severely limited its practical application, especially at elevated temperatures. Relatively, γ-Fe_2O_3 is much more thermodynamically stable and can stand at least 300 °C calcination without any phase transformation, as confirmed in this work. With a special preparation method to form a special morphology, they can even stand calcination at 550−600 °C without phase change.[84] In addition, γ-Fe_2O_3 is ferromagnetic at a wide temperature range which renders it very suitable as catalyst support for easy separation in liquid phase reactions.[85,86] All these features make γ-Fe_2O_3 more applicable as a catalyst support than ferrihydrite, especially for those high-temperature or liquid-phase reactions.

Different from ferrihydrite, γ-Fe_2O_3 itself is less reducible compared with α-Fe_2O_3. However, after incorporation of Au, it was much more reducible than that of α-Fe_2O_3, Figure 5, CO-TPR. A similar trend of H_2-TPR was also observed for Au/α-Fe_2O_3 and Au/γ-Fe_2O_3.[39] Because the size and chemical state of Au were almost same, this different metal-promoting effect must originate from the different metal−support interaction or the special crystal structure of γ-Fe_2O_3. γ-Fe_2O_3 has an inverse spinel structure similar to that of Fe_3O_4 except that it has cation vacancies that compensate for the oxidation of Fe^{II}.[38,67] The same crystal structure allows γ-Fe_2O_3 to be reduced to Fe_3O_4 by loss of O without lattice rearrangement (see Figure S13). The loss of O could occur at low temperature under the assistance of Au species either by H_2/CO spillover or by weakening the strength of the Fe−O band.[19,37] Furthermore, the stronger interaction between Au and γ-Fe_2O_3, as suggested by the less aggregation degree of Au NPs (Figures 3e, f), might activate the Fe−O band in γ-Fe_2O_3 more than that in α-Fe_2O_3. Especially, γ-Fe_2O_3 has cation vacancies which may adsorb metal to form some special/stronger interaction different from that between Au and α-Fe_2O_3, as evidenced by the in situ Raman spectra. As shown in Figure 7, the O species located in the vicinity of cation vacancies was most activated, indicating a stronger/special interaction between gold and these lattice O species. The high activity of Au/γ-Fe_2O_3 clearly suggests that an oxide with high reducibility is not indispensable, as long as the metal/oxide entity has higher reducibility/redox property.

Besides the high activity and the wide application of γ-Fe_2O_3 as a potential support material, this work demonstrated the dramatic effect of crystal phase of iron oxides on CO oxidation activity. It has been noticed recently that CO oxidation on other reducible oxides (for example CeO_2,[31] MnO_x,[32−34] and TiO_2[35,36]) supported Au catalysts also followed the redox mechanism, at a different reaction temperature region and to a different extent. We can therefore in some degree predict the catalytic performance of these oxides-supported metal catalysts on the basis of their reducibility/redox properties. We believe that metal/oxide entity with higher redox property would have higher activity for CO oxidation. Indeed, there is a good example that various single-phase manganese-oxides-supported Au catalysts exhibited a good correlation between their activity for CO oxidation and their reducibility (measured by H_2-TPR), although the highest activity was mainly attributed to the smaller size of Au NPs by the authors.[33] Perhaps the higher redox property is the main origination of the high activity. Apart from CO oxidation, many important chemical reaction were proposed to follow the redox mechanism, such as WGS reaction[75] and selective oxidations which usually use oxides as catalysts.[87] Obviously, an in-depth understanding of the importance of the redox property of oxides-supported noble metal catalysts would be helpful in development of new catalysts or improvement of the catalyst formula. Moreover, recently a correlation between the reducibility of iron oxide crystal phase and the catalytic activity of iron-oxides-supported gold catalysts was also observed for hydrogenation reaction,[88] although their reaction mechanism is different from ours. This suggested that in other types of reaction such as hydrogenation, the catalyst's reducibility also took an important role in determining their catalytic performance, which will make it more valuable to understand the reducibility of the catalysts.

It is worth pointing out that Acerbi et al. recently proposed that the reducibility enhancement of oxides (e.g., CeO_2) by metals depended on the work function[89] and the *d*-band center[90] of the supported metals. This means that we can even predict the reducibility/redox property of metal/oxide and subsequently the activity of metal/oxides catalysts simply by theoretical calculation based on their work function and *d*-band center.

■ CONCLUSIONS

Commercial α-Fe_2O_3- and γ-Fe_2O_3-oxides-supported Au catalysts with identical size of Au NPs, chemical state of Au species and amount of surface OH^- group were prepared. It was found that the Au/γ-Fe_2O_3 catalysts were much more active than Au/α-Fe_2O_3 catalysts for CO oxidation, presenting one of the most active catalysts so far. The high activity originated from the higher redox property of Au/γ-Fe_2O_3, demonstrating that the CO oxidation on Au/γ-Fe_2O_3 mainly followed the redox mechanism. More importantly, this phenomenon could be extended to other γ-Fe_2O_3-supported noble metals and to other reaction that followed redox mechanism. This finding may provide a new avenue for catalyst development by choosing the correct oxide crystal phase.

■ ASSOCIATED CONTENT

Ⓢ Supporting Information

The Supporting Information is available free of charge on the ACS Publications website at DOI: 10.1021/cs5020496.

> Mössbauer parameters of bare γ-Fe_2O_3 and Au/Fe_2O_3 after 300 °C calcination under N_2 atmosphere; XPS spectra of Au4f and O1s of various supported Au catalysts before and after reaction; CO conversion curves for specific rate test and activity comparison of various supported Au catalysts; MS signals of CO and CO_2 for CO-TPR profiles of Au/α-Fe_2O_3−C and Au/γ-Fe_2O_3−C; curves of CO consumption and CO_2 generation during copulse and sequential pulse of CO and O_2 reaction over various supported Au catalysts; TEM images of various supported Pt, Rh, and Au catalysts before or after reaction; in situ DRIFT spectra of various supported Au catalysts under reaction; CO-TPR profiles and CO pulse reactions of supported Pt and Rh catalysts; and crystal structures of various iron oxides (PDF)

■ AUTHOR INFORMATION

Corresponding Authors

*E-mail: wangjh@dicp.ac.cn.
*E-mail: bqiao@dicp.ac.cn.

Present Address

‖(K.Z.) National Engineering Research Center for Nanotechnology, Shanghai, 200241, China.

Author Contributions

#These authors contribute equally to this work (K.Z. and H.T.).

Notes

The authors declare no competing financial interest.

■ ACKNOWLEDGMENTS

This work was supported by the Chinese Academy of Sciences for "100 Talents" Project, National Natural Science Foundation of China (21173218, 21203181, 11079036, 21476232).

■ REFERENCES

(1) Deutschmann, O.; Knözinger, H.; Kochloefl, K.; Turek, T. *Heterogeneous Catalysis and Solid Catalysts*; Wiley-VCH Verlag GmbH & Co. KGaA: Weinheim, Germany, 2000.

(2) Ertl, G.; Knözinger, H.; Schüth, F.; Weitkamp, J. *Handbook of Heterogeneous Catalysis*, 2nd ed.; Wiley-VCH Verlag GmbH& Co. KGaA: Weinheim, Germany, 2008; Vol. *1*.

(3) Norskov, J. K.; Bligaard, T.; Rossmeisl, J.; Christensen, C. H. *Nat. Chem.* **2009**, *1*, 37−46.

(4) Aris, R.; Bell, A. T.; Boudart, M.; Chen, N. Y.; Gates, B. C.; HAAG, W. O.; Somorjar, G. A.; Wei, J. *Catalyst Design: Progress and Perspective*; Wiley-Interscience: New York, 1987.

(5) van Santen, R. A. *Future Perspectives in Catalysis*; Dutch National Research School Combination, Catalysis Controlled by Chemical Design: Eindhoven, Netherlands, 2009.

(6) Derouane, E. G. *CATTECH* **2001**, *5*, 214−225.

(7) Haruta, M. *Chem. Rec.* **2003**, *3*, 75−87.

(8) Hughes, M. D.; Xu, Y.-J.; Jenkins, P.; McMorn, P.; Landon, P.; Enache, D. I.; Carley, A. F.; Attard, G. A.; Hutchings, G. J.; King, F.; Stitt, E. H.; Johnston, P.; Griffin, K.; Kiely, C. J. *Nature* **2005**, *437*, 1132−1135.

(9) Corma, A.; Serna, P. *Science* **2006**, *313*, 332−334.

(10) Turner, M.; Golovko, V. B.; Vaughan, O. P. H.; Abdulkin, P.; Berenguer-Murcia, A.; Tikhov, M. S.; Johnson, B. F. G.; Lambert, R. M. *Nature* **2008**, *454*, 981−983.

(11) Zhong, D.; Franke, J.-H.; Podiyanachari, S. K.; Blömker, T.; Zhang, H.; Kehr, G.; Erker, G.; Fuchs, H.; Chi, L. *Science* **2011**, *334*, 213−216.
(12) Ball, L. T.; Lloyd-Jones, G. C.; Russell, C. A. *Science* **2012**, *337*, 1644−1648.
(13) Finch, R. M.; Hodge, N. A.; Hutchings, G. J.; Meagher, A.; Pankhurst, Q. A.; Siddiqui, M. R. H.; Wagner, F. E.; Whyman, R. *Phys. Chem. Chem. Phys.* **1999**, *1*, 485−489.
(14) Hodge, N. A.; Kiely, C. J.; Whyman, R.; Siddiqui, M. R. H.; Hutchings, G. J.; Pankhurst, Q. A.; Wagner, F. E.; Rajaram, R. R.; Golunski, S. E. *Catal. Today* **2002**, *72*, 133−144.
(15) Qiao, B.; Deng, Y. *Chem. Commun.* **2003**, 2192−2193.
(16) Qiao, B.; Deng, Y. *Appl. Catal., B* **2006**, *66*, 241−248.
(17) Qiao, B.; Zhang, J.; Liu, L.; Deng, Y. *Appl. Catal., A* **2008**, *340*, 220−228.
(18) Qiao, B.; Liu, L.; Zhang, J.; Deng, Y. *J. Catal.* **2009**, *261*, 241−244.
(19) Qiao, B.; Wang, A.; Yang, X.; Allard, L. F.; Jiang, Z.; Cui, Y.; Liu, J.; Li, J.; Zhang, T. *Nat. Chem.* **2011**, *3*, 634−641.
(20) Qiao, B.; Wang, A.; Takahashi, M.; Zhang, Y.; Wang, J.; Deng, Y.; Zhang, T. *J. Catal.* **2011**, *279*, 361−365.
(21) Qiao, B.; Wang, A.; Lin, J.; Li, L.; Su, D.; Zhang, T. *Appl. Catal., B* **2011**, *105*, 103−110.
(22) Lin, J.; Qiao, B.; Liu, J.; Huang, Y.; Wang, A.; Li, L.; Zhang, W.; Allard, L. F.; Wang, X.; Zhang, T. *Angew. Chem., Int. Ed.* **2012**, *51*, 2920−2924.
(23) Liu, L.; Qiao, B.; He, Y.; Zhou, F.; Yang, B.; Deng, Y. *J. Catal.* **2012**, *294*, 29−36.
(24) Qiao, B.; Lin, J.; Li, L.; Wang, A.; Liu, J.; Zhang, T. *ChemCatChem* **2014**, *6*, 547−554.
(25) Golunski, S. *Platinum Met. Rev.* **2013**, *57*, 82−84.
(26) Liu, X.; Liu, M.-H.; Luo, Y.-C.; Mou, C.-Y.; Lin, S. D.; Cheng, H.; Chen, J.-M.; Lee, J.-F.; Lin, T.-S. *J. Am. Chem. Soc.* **2012**, *134*, 10251−10258.
(27) Freund, H. J.; Meijer, G.; Scheffler, M.; Schlogl, R.; Wolf, M. *Angew. Chem., Int. Ed.* **2011**, *50*, 10064−94.
(28) Shelef, M.; McCabe, R. W. *Catal. Today* **2000**, *62*, 35−50.
(29) Twigg, M. V. *Appl. Catal., B* **2007**, *70*, 2−15.
(30) Liu, K.; Wang, A. Q.; Zhang, T. *ACS Catal.* **2012**, *2*, 1165−1178.
(31) Widmann, D.; Leppelt, R.; Behm, R. J. *J. Catal.* **2007**, *251*, 437−442.
(32) Ma, Z.; Liang, C.; Overbury, S. H.; Dai, S. *J. Catal.* **2007**, *252*, 119−126.
(33) Wang, L.-C.; Liu, Q.; Huang, X.-S.; Liu, Y.-M.; Cao, Y.; Fan, K.-N. *Appl. Catal., B* **2009**, *88*, 204−212.
(34) Morgan, K.; Cole, K. J.; Goguet, A.; Hardacre, C.; Hutchings, G. J.; Maguire, N.; Shekhtman, S. O.; Taylor, S. H. *J. Catal.* **2010**, *276*, 38−48.
(35) Widmann, D.; Behm, R. J. *Angew. Chem., Int. Ed.* **2011**, *50*, 10241−10245.
(36) Widmann, D.; Liu, Y.; Schüth, F.; Behm, R. J. *J. Catal.* **2010**, *276*, 292−305.
(37) Li, L.; Wang, A.; Qiao, B.; Lin, J.; Huang, Y.; Wang, X.; Zhang, T. *J. Catal.* **2013**, *299*, 90−100.
(38) Cornell, R. M.; Schwertmann, U. *The Iron Oxides*; Wiley-VCH Verlag GmbH & Co. KGaA: Weinheim, Germany, 2004; pp 9−38.
(39) Huang, J.; Dai, W.-L.; Fan, K. *J. Catal.* **2009**, *266*, 228−235.
(40) Zhao, K.; Qiao, B.; Wang, J.; Zhang, Y.; Zhang, T. *Chem. Commun.* **2011**, *47*, 1779−1781.
(41) Zhao, K.; Qiao, B.; Zhang, Y.; Wang, J. *Chin. J. Catal.* **2013**, *34*, 1386−1394.
(42) Lin, J.; Li, L.; Huang, Y.; Zhang, W.; Wang, X.; Wang, A.; Zhang, T. *J. Phys. Chem. C* **2011**, *115*, 16509−16517.
(43) Wolf, A.; Schuth, F. *Appl. Catal., A* **2002**, *226*, 1−13.
(44) Moreau, F.; Bond, G. C.; Taylor, A. O. *J. Catal.* **2005**, *231*, 105−114.
(45) Haruta, M. *Catal. Today* **1997**, *36*, 153−166.
(46) Valden, M.; Lai, X.; Goodman, D. W. *Science* **1998**, *281*, 1647−1650.
(47) Liu, Y.; Jia, C.-J.; Yamasaki, J.; Terasaki, O.; Schüth, F. *Angew. Chem., Int. Ed.* **2010**, *49*, 5771−5775.
(48) Guzman, J.; Gates, B. C. *J. Am. Chem. Soc.* **2004**, *126*, 2672−2673.
(49) Yu, X.; Hantsche, H. *Fresenius' J. Anal. Chem.* **1993**, *346*, 233−236.
(50) Cuenya, B. R.; Baeck, S.-H.; Jaramillo, T. F.; McFarland, E. W. *J. Am. Chem. Soc.* **2003**, *125*, 12928−12934.
(51) Cornell, R. M.; Schwertmann, U. *The Iron Oxides*; Wiley-VCH Verlag GmbH & Co. KGaA: Weinheim, Germany, 2004; pp 111−137.
(52) Peters, S.; Peredkov, S.; Neeb, M.; Eberhardt, W.; Al-Hada, M. *Surf. Sci.* **2013**, *608*, 129−134.
(53) Costello, C. K.; Kung, M. C.; Oh, H. S.; Wang, Y.; Kung, H. H. *Appl. Catal., A* **2002**, *232*, 159−168.
(54) Smit, G.; Strukan, N.; Craje, M. W. J.; Lazard, K. *J. Mol. Catal. A: Chem.* **2006**, *252*, 163−170.
(55) Veith, Gabriel M.; Lupini, Andrew R.; Pennycook, Stephen J.; Dudney, Nancy J. *ChemCatChem.* **2010**, *2*, 281−286.
(56) Herzing, A. A.; Kiely, C. J.; Carley, A. F.; Landon, P.; Hutchings, G. J. *Science* **2008**, *321*, 1331−1335.
(57) Jing, L. Q.; Wang, D. J.; Wang, B. Q.; Li, S. D.; Xin, B. F.; Fu, H. G.; Sun, J. Z. *J. Mol. Catal. A: Chem.* **2006**, *244*, 193−200.
(58) Haber, J.; Stoch, J.; Ungier, L. *J. Electron Spectrosc. Relat. Phenom.* **1976**, *9*, 459−467.
(59) Martensson, N.; Malmquist, P. A.; Svensson, S.; Basilier, E.; Pireaux, J. J.; Gelius, U.; Siegbahn, K. *Nouveau, J. Chim.* **1977**, *1*, 191−195.
(60) Carabineiro, S. A. C.; Bogdanchikova, N.; Tavares, P. B.; Figueiredo, J. L. *RSC Adv.* **2012**, *2*, 2957−2965.
(61) Schüth, F. *Phys. Status Solidi B* **2013**, *250*, 1142−1151.
(62) Haruta, M. *Faraday Discuss.* **2011**, *152*, 11−32.
(63) Chen, M.; Goodman, D. W. *Science* **2004**, *306*, 252−255.
(64) Li, P.; Miser, D. E.; Rabiei, S.; Yadav, R. T.; Hajaligol, M. R. *Appl. Catal., B* **2003**, *43*, 151−162.
(65) Zielinski, J.; Zglinicka, I.; Znak, L.; Kaszkur, Z. *Appl. Catal., A* **2010**, *381*, 191−196.
(66) Legodi, M. A.; de Waal, D. *Dyes Pigm.* **2007**, *74*, 161−168.
(67) Long, J. W.; Logan, M. S.; Rhodes, C. P.; Carpenter, E. E.; Stroud, R. M.; Rolison, D. R. *J. Am. Chem. Soc.* **2004**, *126*, 16879−16889.
(68) de Faria, D. L. A.; Venâncio Silva, S.; de Oliveira, M. T. *J. Raman Spectrosc.* **1997**, *28*, 873−878.
(69) Corti, C. W.; Holliday, R. J.; Thompson, D. T. *Top. Catal.* **2007**, *44*, 331−343.
(70) Fierro-Gonzalez, J. C.; Gates, B. C. *J. Phys. Chem. B* **2004**, *108*, 16999−17002.
(71) Mihaylov, M.; Knözinger, H.; Hadjiivanov, K.; Gates, B. C. *Chem. Ing. Tech.* **2007**, *79*, 795−806.
(72) Ligthart, D. A. J. M.; van Santen, R. A.; Hensen, E. J. M. *Angew. Chem., Int. Ed.* **2011**, *50*, 5306−5310.
(73) Grass, M. E.; Zhang, Y. W.; Butcher, D. R.; Park, J. Y.; Li, Y. M.; Bluhm, H.; Bratlie, K. M.; Zhang, T. F.; Somorjai, G. A. *Angew. Chem., Int. Ed.* **2008**, *47*, 8893−8896.
(74) Ghosh, T. K.; Nair, N. N. *ChemCatChem* **2013**, *5*, 1811−1821.
(75) Ratnasamy, C.; Wagner, J. P. *Catal. Rev.: Sci. Eng.* **2009**, *51*, 325−440.
(76) Andreeva, D.; Idakiev, V.; Tabakova, T.; Andreev, A.; Giovanoli, R. *Appl. Catal., A* **1996**, *134*, 275−283.
(77) Boccuzzi, F.; Chiorino, A.; Manzoli, M.; Andreeva, D.; Tabakova, T. *J. Catal.* **1999**, *188*, 176−185.
(78) Aeijelts Averink Silberova, B.; Mul, G.; Makkee, M.; Moulijn, J. A. *J. Catal.* **2006**, *243*, 171−182.
(79) Kozlova, A. P.; Sugiyama, S.; Kozlov, A. I.; Asakura, K.; Iwasawa, Y. *J. Catal.* **1998**, *176*, 426−438.
(80) Smit, G. *Croat. Chem. Acta* **2003**, *76*, 269−271.
(81) Gawande, M. B.; Rathi, A. K.; Tucek, J.; Safarova, K.; Bundaleski, N.; Teodoro, O. M. N. D.; Kvitek, L.; Varma, R. S.; Zboril, R. *Green Chem.* **2014**, *16*, 4137−4143.

(82) Cornell, R. M.; Schwertmann, U. *The Iron Oxides*; Wiley-VCH Verlag GmbH & Co. KGaA: Weinheim, Germany, 2004; pp 1−7.

(83) Golunski, S.; Rajaram, R.; Hodge, N.; Hutchings, G. J.; Kiely, C. J. *Catal. Today* **2002**, *72*, 107−113.

(84) Mou, X.; Zhang, B.; Li, Y.; Yao, L.; Wei, X.; Su, D. S.; Shen, W. *Angew. Chem., Int. Ed.* **2012**, *51*, 2989−2993.

(85) Mori, K.; Kanai, S.; Hara, T.; Mizugaki, T.; Ebitani, K.; Jitsukawa, K.; Kaneda, K. *Chem. Mater.* **2007**, *19*, 1249−1256.

(86) Mou, X.; Wei, X.; Li, Y.; Shen, W. *CrystEngComm* **2012**, *14*, 5107−5120.

(87) Mars, P.; van Krevelen, D. W. *Chem. Eng. Sci.* **1954**, *3* (Supplement 1), 41−59.

(88) Milone, C.; Crisafulli, C.; Ingoglia, R.; Schipilliti, L.; Galvagno, S. *Catal. Today* **2007**, *122*, 341−351.

(89) Acerbi, N.; Tsang, S. C.; Golunski, S.; Collier, P. *Chem. Commun.* **2008**, *0*, 1578−1580.

(90) Acerbi, N.; Tsang, S. C. E.; Jones, G.; Golunski, S.; Collier, P. *Angew. Chem., Int. Ed.* **2013**, *52*, 7737−7741.